ENCIT 2018

ABCM Associação Brasileira de Engenharia e Ciências Mecânicas

17th Brazilian Congress of Thermal Sciences and Engineering
November 25th-28th, 2018, Águas de Lindóia, SP, Brazil

ENCIT-2018-0814
Application of Deep Learning and Proper Orthogonal Decomposition for Reduced Order Models of Unsteady Flows

Hugo F. S. Lui
William R. Wolf
Universidade Estadual de Campinas, UNICAMP, 13083-970 Campinas, SP, Brazil
hugo.slui@gmail.com
wolf@fem.unicamp.br

Abstract. *In this work, we present a numerical methodology which combines flow modal decomposition via proper orthogonal decomposition and sparse regression using deep neural networks. The framework is implemented in the context of the sparse identification of non-linear dynamics algorithm recently proposed in the literature. The framework is applied for the construction of reduced order models of unsteady compressible flows. The results demonstrate that the technique provides accurate and stable reconstructions of the full order model beyond the training window of the deep neural network. In this paper, we describe the numerical techniques employed and show the results obtained by the current methodology.*

Keywords: *Reduced Order Models, Deep Learning, Proper Orthogonal Decomposition, Computational Fluid Dynamics*

1. INTRODUCTION

Current supercomputers allow the application of high fidelity numerical simulations of turbulent flows over large scale industrial configurations. These simulations may lead to discretizations with billions of degrees of freedom in order resolve the energetically relevant spatial scales. Moreover, the fluid flow data needs to be recorded for long periods using small time steps to compute converged statistics of the flow with sufficient accuracy.

The results from large scale computations certainly improve the understanding of several physical mechanisms such as mixing enhancement, drag reduction, heat transfer, noise generation, to name a few. At the same time, high fidelity calculations require the acquisition and treatment of large databases which introduces a big data challenge. In recent years, novel data-driven algorithms have been developed and applied to perform statistical post-processing of large databases of unsteady fluid flows. For example, one can cite techniques of flow modal decomposition (Taira *et al.*, 2017) such as proper orthogonal decomposition (POD) (Lumley, 1967; Sieber *et al.*, 2016; Ribeiro and Wolf, 2017), dynamic mode decomposition (DMD) (Schmid, 2010), and Lagrangian coherent structures (LCS) (Haller, 2015).

In order to reduce the computational costs from large scale flow simulations, reduced order models (ROM) need to be developed for application in the preliminary stages of design. Such tools should be also useful for optimization and flow control. Several ROM techniques have been discussed in the literature such as Galerkin projection (Rowley *et al.*, 2004), balanced truncation Galerkin projection (Carlberg *et al.*, 2015), eigensystem realization analysis (Juang and Pappa, 1985) and sparse regression of nonlinear dynamics (Brunton *et al.*, 2016). These techniques have been mostly applied for canonical problems and their application in turbulent flows over industrial configurations is still a challenging task.

Machine learning is a possible candidate for the development of accurate and stable ROMs for industrial configurations. In this work, we present a numerical methodology which combines flow modal decomposition via POD and sparse regression using machine learning and deep neural networks (DNN) (Goodfellow *et al.*, 2016; Glorot and Bengio, 2010; Kutz, 2017). The framework is implemented in the context of the sparse identification of non-linear dynamics (SINDy) algorithm (Brunton *et al.*, 2016). The framework is applied for the construction of ROMs of unsteady compressible flows involving noise generation and propagation. In this paper, we describe the numerical techniques employed and show the results obtained by the current methodology.

2. FLOW SIMULATION

In this work, the compressible Navier-Stokes equations are solved in their covariant form on a general curvilinear system. The numerical scheme for spatial discretization is a sixth-order accurate compact scheme (Nagarajan *et al.*, 2003) implemented on a staggered grid. A sixth-order compact scheme is also employed for interpolation (Lele, 1992) of fluid properties on the different nodes of the staggered configuration. Compact finite-difference schemes are non-dissipative and numerical instabilities arising from mesh non-uniformities and approximate boundary conditions have to be filtered

to preserve stability of the numerical schemes. The high wavenumber compact filter presented by Lele (1992) is applied to the computed solution at prescribed time intervals in order to control numerical instabilities. This filter is only applied in flow regions far away from solid boundaries.

The time integration of the fluid equations is carried out by the fully implicit second-order scheme of Beam and Warming (Beam, 1978) in the near-wall region in order to overcome the time step restriction due to the usual near-wall fine-grid numerical stiffness. A third-order Runge-Kutta scheme is used for time advancement of the equations in flow regions far away from solid boundaries. No-slip adiabatic wall boundary conditions are applied along the solid surfaces and characteristic plus sponge boundary conditions are applied in the far field locations. The numerical tool has been previously validated for several simulations of unsteady compressible flows (Wolf *et al.*, 2012b,a; Arias Ramirez and Wolf, 2015).

3. FORMULATION

The equations governing an unsteady two-dimensional compressible flow contain partial derivatives with respect to both space $\mathbf{x} = [x, y]^T$ and time t. Using the method of lines one can approximate the spatial derivatives first, producing a system of nonlinear ordinary differential equations (ODEs). In the most general notation, for each mesh point, these ODEs would be expressed in the form

$$\frac{d\mathbf{q}}{dt} = \mathbf{F}(\mathbf{q}, t) \,, \tag{1}$$

where $\mathbf{F}$ is a nonlinear operator, $\mathbf{q} = [\rho, \rho u, \rho v, E]^T$ is the vector of conservative variables, ρ is the density, u is the x-component of the velocity vector, v is the y-component of the velocity vector and E is the total energy per unit of volume.

We can consider each mesh point as a dynamical system of form Eq. (1). To determine the function $\mathbf{F}$ from data, we use the sparse identification of nonlinear dynamics algorithm (SINDy) developed by Brunton *et al.* (2016) with some modifications. First, we collect snapshots of the conservative variables $(\rho, \rho u, \rho v, E)$ which will be our training data. For each conservative variable, the data set is arranged into a matrix $\mathbf{Q}$ as

$$\mathbf{Q} = \begin{bmatrix} \mathbf{q}(\mathbf{x_1}, t_1) & \mathbf{q}(\mathbf{x_2}, t_1) & \dots & \mathbf{q}(\mathbf{x_{N_p}}, t_1) \\ \mathbf{q}(\mathbf{x_1}, t_2) & \mathbf{q}(\mathbf{x_2}, t_2) & \dots & \mathbf{q}(\mathbf{x_{N_p}}, t_2) \\ \vdots & \vdots & \ddots & \vdots \\ \mathbf{q}(\mathbf{x_1}, t_{N_T}) & \mathbf{q}(\mathbf{x_2}, t_{N_T}) & \dots & \mathbf{q}(\mathbf{x_{N_p}}, t_{N_T}) \end{bmatrix} \tag{2}$$

where N_p is the number of grid points in the computational domain and N_T is the number of snapshots.

Because of the high dimensionality of the input data $\mathbf{Q}$, it is first necessary to reduce the dimension of the dynamical system. The proper orthogonal decomposition (POD) has been widely used to obtain optimal bases that represent the most energetic content of the system dynamics with as few bases functions as possible (Lumley, 1967; Sieber *et al.*, 2016). In the following derivations, the vector notation will be implicitly assumed. The snapshot POD approach starts with a decomposition of the vector quantities $q(\mathbf{x}, t)$ into the mean flow, $\overline{q}(\mathbf{x})$, and fluctuations, $q'(\mathbf{x}, t)$. The latter can be further expanded into a combination of spatial modes $\phi_i(\mathbf{x})$ and their temporal coefficients $a_i(t)$ for a defined number of N modes as

$$q(\mathbf{x}, t) = \overline{q}(\mathbf{x}) + q'(\mathbf{x}, t) = \overline{q}(\mathbf{x}) + \sum_{i=1}^{N} a_i(t)\phi_i(\mathbf{x}) \,. \tag{3}$$

To calculate the POD correlation matrix of the data set $\mathbf{Q}$ some specific norm must be used. For an incompressible flow, a kinetic energy norm provides an optimal result, however, for a compressible flow, other norms can be employed (Rowley *et al.*, 2004). Hence, the correlation between two snapshots is calculated from a L^2 inner product $\langle \, , \rangle$. The elements of the correlation matrix $\mathbf{C}$ are given by

$$C_{ij} = \langle \, q'(\mathbf{x}, t_i), q'(\mathbf{x}, t_j) \rangle \,, \tag{4}$$

and the matrix C is of size $N \times N$. The temporal coefficients $\mathbf{a_i} = [a_i(t_1), ..., a_i(t_{N_T})]^T$ and the mode energies λ_i are determined from the eigenvectors and eigenvalues of the correlation matrix $\mathbf{C}$ as

$$\mathbf{C}\mathbf{a_i} = \lambda_i \mathbf{a_i} \,. \tag{5}$$

Here, singular value decomposition (SVD) can be employed to compute the eigenvalues λ_i and eigenvectors $\mathbf{a_i}$ of $\mathbf{C}$ since the matrix is real symmetric positive-definite. The spatial modes are obtained from the projection of the fluctuation quantities onto the temporal coefficients

$$\phi_i(\mathbf{x}) = \frac{1}{\lambda_i} \sum_{j=1}^{N} a_i(t_j) q'(\mathbf{x}, t_j) \,. \tag{6}$$

Finally, the temporal coefficients and spatial modes can be stored in matrices $\mathbf{A}$ and $\mathbf{\Phi}$ as

$$\mathbf{A} = \begin{bmatrix} \mathbf{a}^T(t_1) \\ \mathbf{a}^T(t_2) \\ \vdots \\ \mathbf{a}^T(t_{N_T}) \end{bmatrix} = \begin{bmatrix} a_1(t_1) & a_2(t_1) & ... & a_N(t_1) \\ a_1(t_2) & a_2(t_2) & ... & a_N(t_2) \\ \vdots & \vdots & \ddots & \vdots \\ a_1(t_{N_T}) & a_2(t_{N_T}) & ... & a_N(t_{N_T}) \end{bmatrix} \tag{7}$$

and

$$\mathbf{\Phi} = \begin{bmatrix} \phi_1(\mathbf{x_1}) & \phi_1(\mathbf{x_2}) & ... & \phi_1(\mathbf{x}_{N_p}) \\ \phi_2(\mathbf{x_1}) & \phi_2(\mathbf{x_2}) & ... & \phi_2(\mathbf{x}_{N_p}) \\ \vdots & \vdots & \ddots & \vdots \\ \phi_N(\mathbf{x_1}) & \phi_N(\mathbf{x_2}) & ... & \phi_N(\mathbf{x}_{N_p}) \end{bmatrix}, \tag{8}$$

where the temporal coefficients are the columns of $\mathbf{A}$ and the spatial modes are the rows of $\mathbf{\Phi}$.

Taking the time derivative of Eq. (3), we arrive at the following equation

$$\frac{d\mathbf{q}(t)}{dt} = \sum_{i=1}^{N} \phi_i(\mathbf{x}) \frac{da_i(t)}{dt} \, . \tag{9}$$

The last term of Eq. (9) represents the temporal evolution of coefficients $a_i(t)$ associated with N modes retained in the POD basis. We can express this system of coupled ODEs as

$$\frac{d\mathbf{a}(t)}{dt} = \dot{\mathbf{a}}(t) = \mathbf{F}(\mathbf{a}(t)) \, . \tag{10}$$

Next, we compute the derivative $\dot{\mathbf{a}}(t)$ numerically using the data $\mathbf{a}(t)$ for each temporal mode. The numerical scheme employed is a 10th-order accurate compact scheme (Lele, 1992) which provides high spectral resolution being non-dissipative and low-dispersive. The derivatives $\dot{\mathbf{a}}(t)$ are then arranged into a matrix $\dot{\mathbf{A}}$

$$\dot{\mathbf{A}} = \begin{bmatrix} \dot{\mathbf{a}}^T(t_1) \\ \dot{\mathbf{a}}^T(t_2) \\ \vdots \\ \dot{\mathbf{a}}^T(t_{N_T}) \end{bmatrix} = \begin{bmatrix} \dot{a}_1(t_1) & \dot{a}_2(t_1) & ... & \dot{a}_N(t_1) \\ \dot{a}_1(t_2) & \dot{a}_2(t_2) & ... & \dot{a}_N(t_2) \\ \vdots & \vdots & \ddots & \vdots \\ \dot{a}_1(t_{N_T}) & \dot{a}_2(t_{N_T}) & ... & \dot{a}_N(t_{N_T}) \end{bmatrix} . \tag{11}$$

Now, we may set up a regression problem to find the weights $\mathbf{W} = [\mathbf{w}_1 \; \mathbf{w}_2 \; ... \; \mathbf{w}_N]$ and biases $\mathbf{b} = [b_1, b_2, ..., b_N]^T$ that determine the function $F(\mathbf{a}(t))$ presented in Eq. (10)

$$\dot{\mathbf{A}} = \mathbf{W}\mathbf{\Theta}(\mathbf{A}) + \mathbf{b} \, , \tag{12}$$

where $\mathbf{w}_i$ is a vector of weights and $\mathbf{\Theta}(\mathbf{A})$ is matrix of features.

Brunton *et al.* (2016) suggest that $\mathbf{\Theta}(\mathbf{A})$ may consist of constant, polynomial, exponential and trigonometric functions. However, in many cases, it is complicated to know what set of features should be extracted from the data. Hence, we try to circumvent the problem of finding the functions which represent the dynamics of the problem using machine learning to discover not only the weights $\mathbf{W}$ and biases $\mathbf{b}$ but also the features $\mathbf{\Theta}(\mathbf{A})$. The "learned" features often result in a better performance than can those obtained using "engineered" features. A learning algorithm can find a good set of features in minutes or hours, depending on the task complexity. However, manually engineered features would require a great amount of human time and effort for complex tasks (Goodfellow *et al.*, 2016).

Deep learning methods are feature learning algorithms. These methods aim at learning a good set of features, often at multiple layers, from higher layer features defined in terms of lower layer features. Automatically learning features at multiple processing layers allow systems to learn complex functions through mapping the input to the output directly from a given data (Bengio, 2009). Here, a standard deep feedforward network (DNN) (Goodfellow *et al.*, 2016) is used to learn the weights $\mathbf{W}$, biases $\mathbf{b}$ and features $\mathbf{\Theta}(\mathbf{A})$.

Figure 1 shows a sample DNN arquitecture where the input $\mathbf{X}$ of the DNN is the matrix $\mathbf{A}$ and the target $\mathbf{Y}$ is the matrix $\dot{\mathbf{A}}$. The weights $\mathbf{W}^{[l]}$ are initialized using Xavier initialization (Glorot and Bengio, 2010). The biases $\mathbf{b}^{[l]}$ are initialized to zero. The matrix $\mathbf{W}^{[l]}$ is of size $n^{[l+1]} \times n^{[l]}$ and the vector $\mathbf{b}^{[l]}$ is of size $n^{[l]} \times 1$, where l is the l-th layer. For all hidden layers expect the last, the activation function $G^{[l]}$ is the $\tanh$, while for the last layer, we employ a linear function. The cost function is the mean squared error (MSE), which measures the difference between the training samples and the predictions. In order to find the parameters $\mathbf{W}^{[l]}$ and $\mathbf{b}^{[l]}$ of the deep neural network that significantly reduce the cost function, we use ADAM optimizer, (Kingma and Ba, 2014). The optimization process requires a set of hyperparameters: learning rate α, regularization parameter λ, maximum number of iterations n_{iter}, the exponential decay

rate for the 1st moment estimates β_1, the exponential decay rate for the 2nd moment estimates β_2 and a small constant for numerical stability ϵ. The hyperparameters are set with a random grid search. In the current work, the open source machine learning framework Tensorflow (Abadi *et al.*, 2015) is used for training the DNN.

Once we have learned the parameters $\mathbf{W}^{[l]}$ and $\mathbf{b}^{[l]}$ of our model Eq. (12), we can use them to predict the temporal coefficients a_i given the initial conditions $\mathbf{a}^T(t_1)$. The system of coupled ODEs is integrated using an explicit 5 stage 4th-order Runge-Kutta scheme derived by Kennedy *et al.* (1999). As we have the temporal coefficients $\mathbf{a}(t)$, one can reconstruct the flowfield using Eq. (3). However, we are interested in using a reduced order model in circumstances other than simply reproducing the training data. The approach presented in this work allows to predict the flowfield beyond the training window as $\overline{q}(\mathbf{x})$ and $\phi(\mathbf{x})$ depend only on the spatial coordinates $\mathbf{x}$.

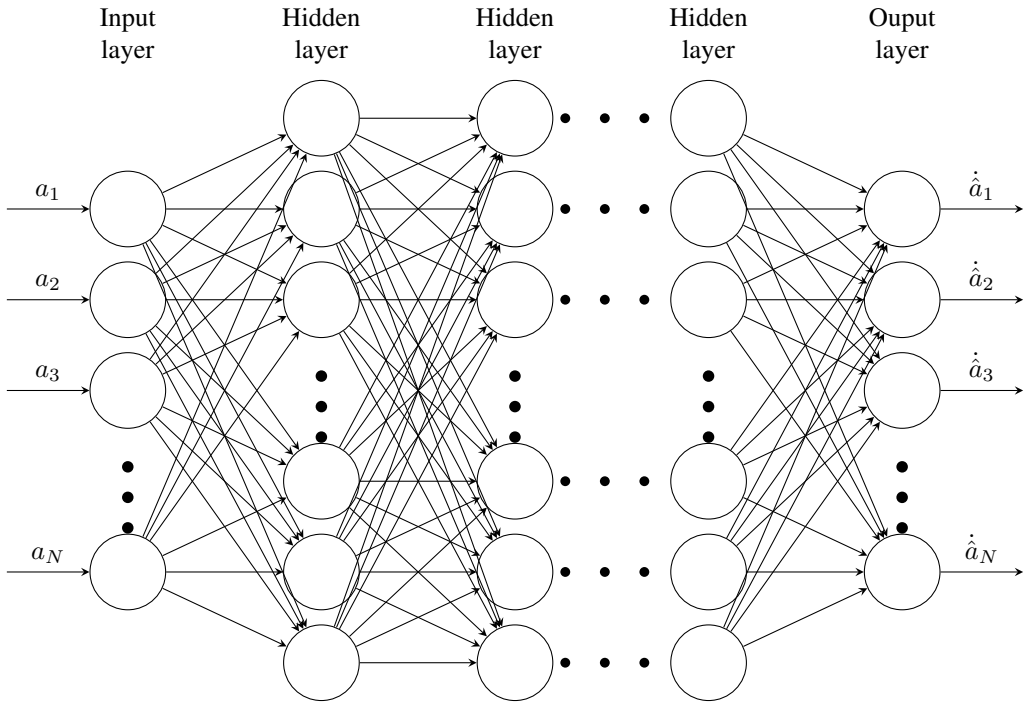

Figure 1. An example of a deep neural network with N inputs, many hidden layers (HL), and a output layer with N outputs.

4. RESULTS

This section presents the results obtained by the algorithm proposed here which combines sparse regression, POD and deep learning. In this paper, the reduced order model is employed to reconstruct simulations of a two-dimensional compressible flow past a cylinder. The full order model (FOM) is obtained by solving the compressible Navier Stokes equations as detailed in section 2. The numerical simulations are conducted for Reynolds and Mach numbers Re = 150 and M = 0.4, respectively. These non-dimensional parameters are computed based on freestream quantities. The grid configuration consists of a body-fitted O-grid of with 421 × 751 points in the streamwise and wall-normal direction, respectively.

The flow is recorded for 1120 snapshots with non-dimensional time steps of h = 0.05. These snapshots are collected after an initial transient period of the simulation is discarded. The reduced order model is obtained following the procedures described in section 3. The training data comprises the first 620 snapshots of the FOM and the remaining data is the test set. The details of the architecture of the deep neural network are shown in Tab. 1 and the hyperparameters employed in the algorithm described in the previous section are presented in Tab. 2.

Table 1. DNN architecture

	Input layer	HL 1	HL 2	HL 3	HL 4	HL 5	HL 6	HL 7	Output Layer
# of hidden units	12	24	20	18	16	16	16	16	12

Figures 2 to 5 show contours of density, x and y-momentum, and z-vorticity, respectively, along the cylinder and wake regions at time t = 409.025, which is beyond the training window. The snapshots compare the results between the full

Table 2. Hyperparameters

α	λ	n_{iter}	β_1	β_2	ϵ
0.0005	0.000045	10000	0.9	0.999	1.0×10^{-8}

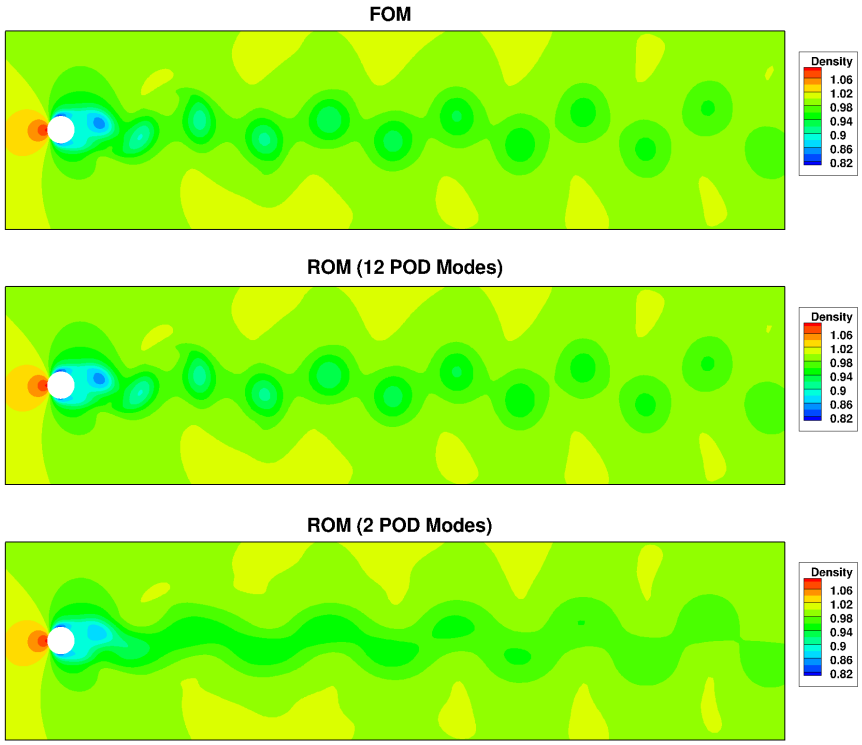

Figure 2. Contours of density, $\mathbf{t} = \mathbf{409.025}$

order model and the reduced order model using 2 and 12 POD modes out of 620 modes. Hence, the flow is reconstructed using 0.3% and 2% of the total information available from the full order model. Reconstruction of the individual flow variables with 2 POD modes could recover between 50 and 80% of the total energy of the modes, depending on the variable (for example, density is reconstructed using 50% of the total energy of the modes while y-momentum is reconstructed with 80%). For 12 POD modes, the reconstructions could recover 99% of the energy and, therefore, should lead to good flow representations.

One can observe from the figures that the computations of the flow using the ROM framework show good agreement with those obtained by the full order numerical simulation. For the current Reynolds number, the flow develops a typical von Kármán vortex street along the cylinder wake. The periodical pattern of the vortex shedding can be observed in the figures, in particular for the vorticity and y-momentum contours. When 2 POD modes are employed in the flow reconstruction, discrepancies between the ROM and FOM are evident from the figures. However, the main features of the flow are still recovered by the model, especially for the x-momentum solution. One should remind that, despite the use of only 2 modes, the dynamical system is still stable. In fact, the regression via DNN is even more efficient for this case since the POD temporal modes show a simpler behavior than those for higher order POD modes. The reconstruction using 12 POD modes show an excellent agreement with the FOM.

In order to show a more qualitative evaluation of the model reconstructions, the density, x-momentum and y-momentum fluctuation time histories are presented for the FOM and ROMs in Figs. 6 to 8. The figures on the left column show results for a probe located just behind the cylinder, close to the surface. On the right column, results are obtained for a probe downstream the cylinder wake. Results are shown for both the training window period and beyond. When 2 POD modes are employed, the solutions show a poor representation of the dynamics observed in the FOM. The density reconstruction is that with the highest discrepancy and that is attributed to the lower energetic content achieved by the first 2 modes. The reconstructions show a better comparison with the FOM just behind the cylinder. For the y-momentum, the reconstruction with 2 POD modes shows a better agreement for both probe locations. One can notice that the reduced order model accurately reproduces the full order model results during and beyond the training window when 12 POD modes are employed in the reconstruction.

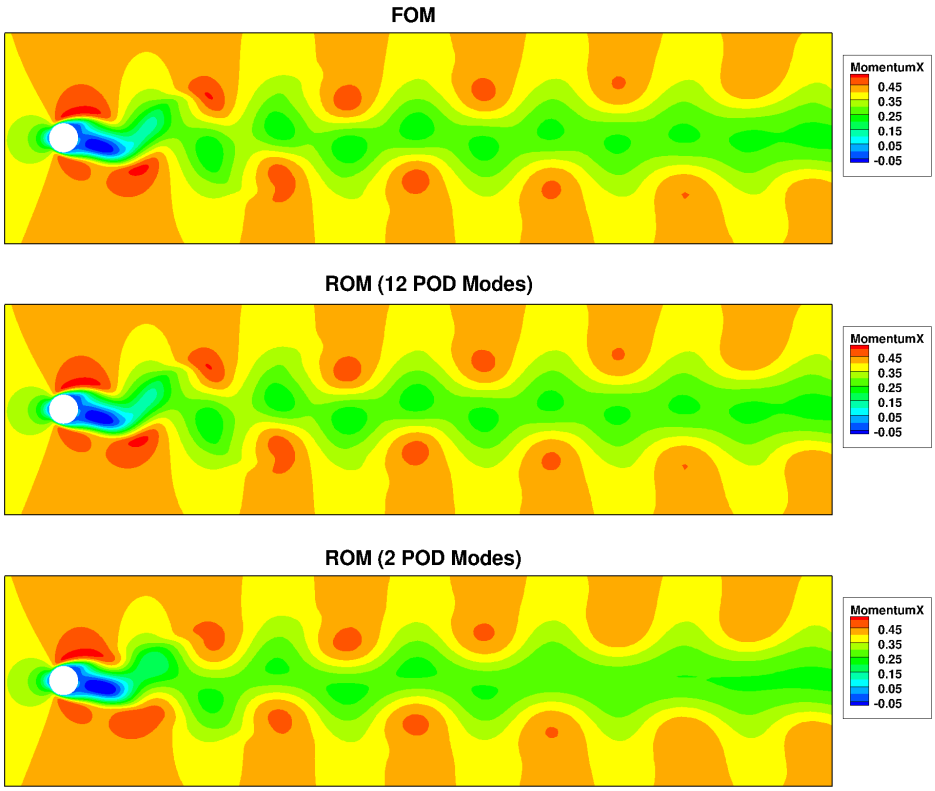

Figure 3. Contours of $\mathbf{x}$-momentum, $\mathbf{t}$ = $\mathbf{409.025}$

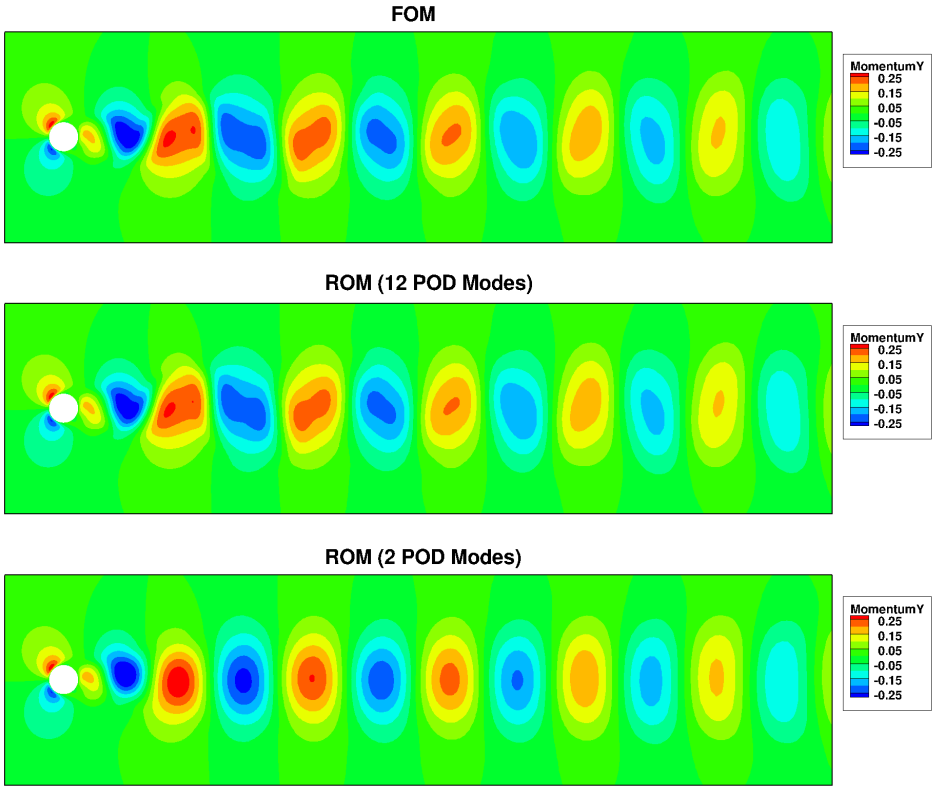

Figure 4. Contours of $\mathbf{y}$-momentum, $\mathbf{t}$ = $\mathbf{409.025}$

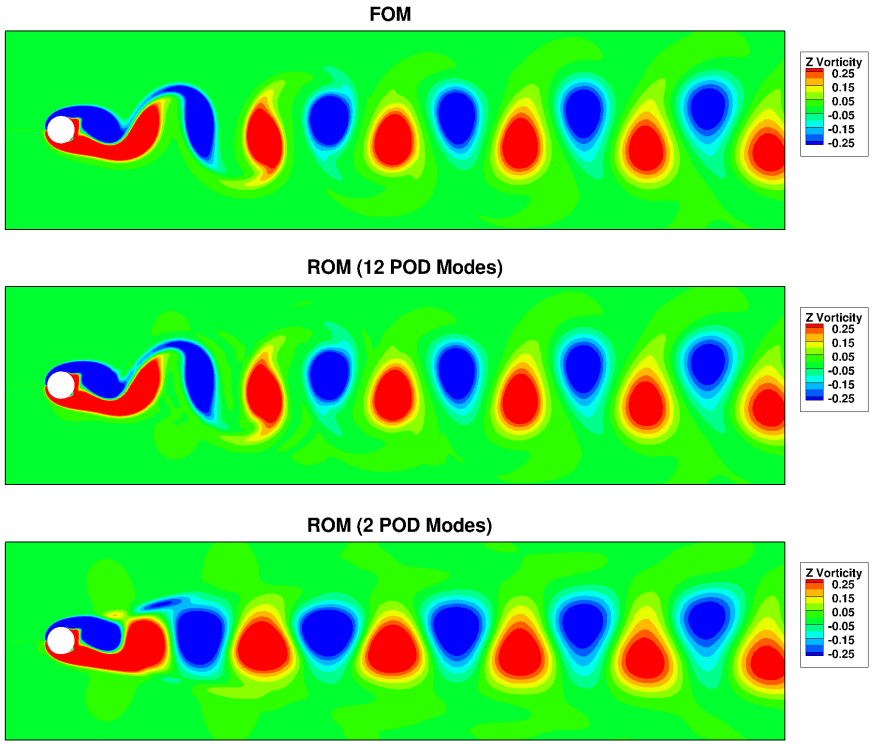

Figure 5. Contours of z-vorticity, $\mathbf{t} = \mathbf{409.025}$

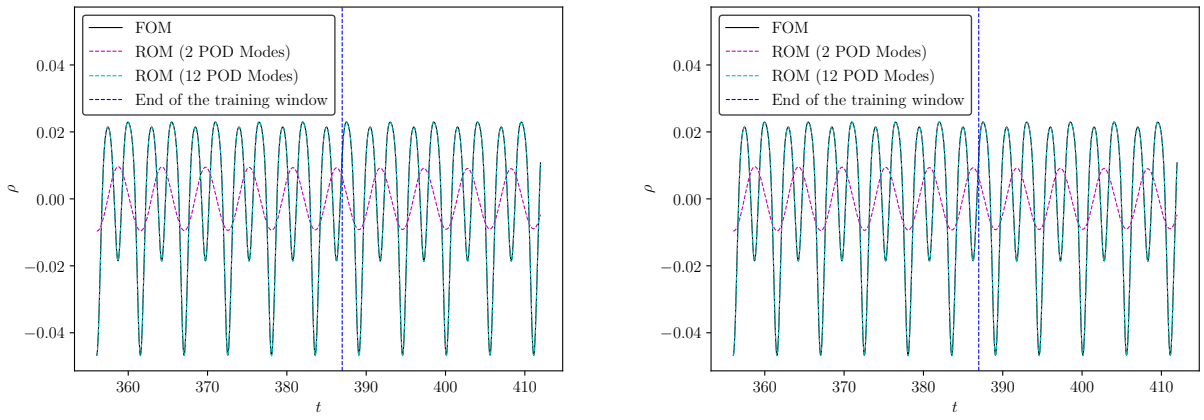

(a) Probe just behind the cylinder.

(b) Probe away from the cylinder, along the wake.

Figure 6. Fluctuation time history of density for probes located at different positions.

5. CONCLUSIONS

In the present work we present a methodology for constructing reduced order models combining flow modal decomposition, sparse regression and deep learning. The framework is implemented in the context of the sparse identification of non-linear dynamics (SINDy) algorithm recently proposed in the literature. Numerical simulations are performed using a high-order compact finite difference flow solver to provide the database for the construction of the reduced order model. In this paper, the compressible Navier Stokes equations are solved for the flow past a cylinder. We first perform a proper orthogonal decomposition (POD) of the flow and, then, a sparse regression of the POD temporal modes is conducted using deep neural networks.

The results demonstrate that the technique provides accurate reconstructions of the full order model provided by the solution of the Navier Stokes equations. The method provides stable solutions even beyond the training window of the deep neural network. In this paper, we describe the numerical techniques employed and show the results obtained by the current methodology.

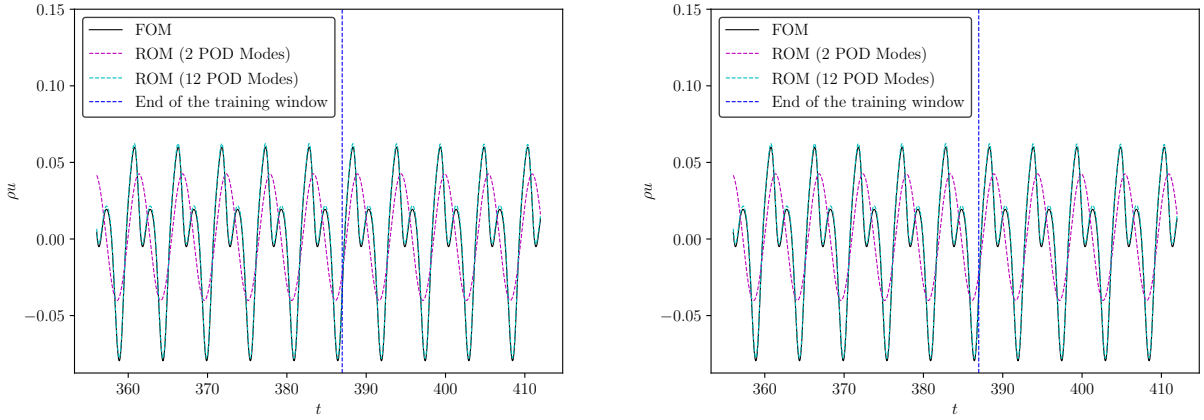

(a) Probe just behind the cylinder.

(b) Probe away from the cylinder, along the wake.

Figure 7. Fluctuation time history of x-momentum for probes located at different positions.

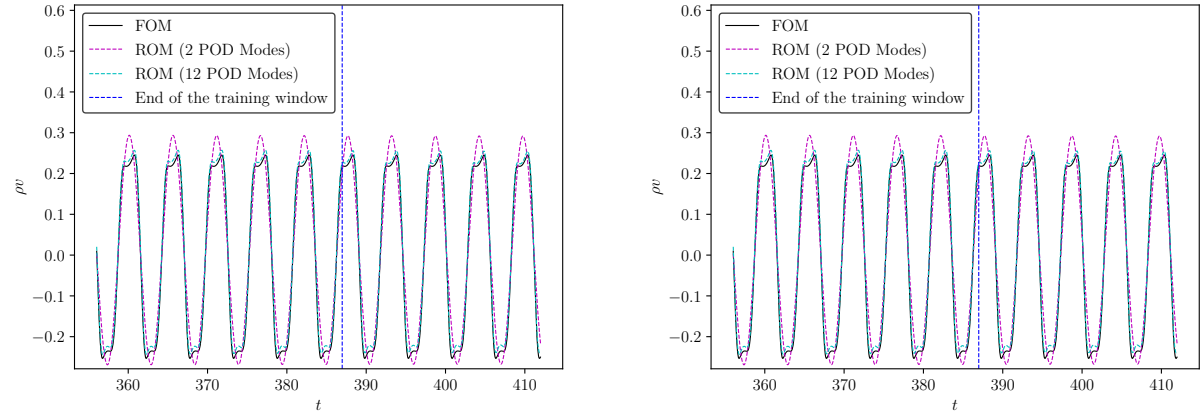

(a) Probe just behind the cylinder.

(b) Probe away from the cylinder, along the wake.

Figure 8. Fluctuation time history of y-momentum for probes located at different positions.

6. ACKNOWLEDGEMENTS

The work is partially supported by Fundação de Amparo à Pesquisa do Estado de São Paulo, FAPESP, under Research Grants No. 2013/07375-0 and No. 2013/03413-4. The support provided by Coordenação de Aperfeiçoamento de Pessoal de Nível Superior, CAPES, through a scholarship for the first author is likewise gratefully appreciated.

7. REFERENCES

Abadi, M., Agarwal, A., Barham, P., Brevdo, E., Chen, Z., Citro, C., Corrado, G.S., Davis, A., Dean, J., Devin, M., Ghemawat, S., Goodfellow, I., Harp, A., Irving, G., Isard, M., Jia, Y., Jozefowicz, R., Kaiser, L., Kudlur, M., Levenberg, J., Mané, D., Monga, R., Moore, S., Murray, D., Olah, C., Schuster, M., Shlens, J., Steiner, B., Sutskever, I., Talwar, K., Tucker, P., Vanhoucke, V., Vasudevan, V., Viégas, F., Vinyals, O., Warden, P., Wattenberg, M., Wicke, M., Yu, Y. and Zheng, X., 2015. "TensorFlow: Large-scale machine learning on heterogeneous systems". URL `https://www.tensorflow.org/`. Software available from tensorflow.org.

Arias Ramirez, W. and Wolf, W.R., 2015. "Effects of trailing edge bluntness on airfoil tonal noise at low reynolds numbers". *Journal of the Brazilian Society of Mechanical Sciences and Engineering*. ISSN 1678-5878.

Beam, R. M.and Warming, R.F., 1978. "An implicit factored scheme for the compressible navier-stokes equations". *AIAA Journal*, Vol. 16, No. 4, pp. 393–402. ISSN 0001-1452.

Bengio, Y., 2009. "Learning deep architectures for ai". *Found. Trends Mach. Learn.*, Vol. 2, No. 1, pp. 1–127. ISSN 1935-8237.

Brunton, S.L., Proctor, J.L. and Kutz, J.N., 2016. "Discovering governing equations from data by sparse identification of nonlinear dynamical systems". Vol. 113, No. 15, pp. 3932–3937.

Carlberg, K., Bou-Mosleh, C. and Farhat, C., 2015. "Efficient non-linear model reduction via a least-squares petrov-galerkin projection and compressive tensor approximations". *International Journal for Numerical Methods in Engineering*, Vol. 86, pp. 155–181.

Glorot, X. and Bengio, Y., 2010. "Understanding the difficulty of training deep feedforward neural networks". In *Proceedings of the Thirteenth International Conference on Artificial Intelligence and Statistics, AISTATS 2010, Chia Laguna Resort, Sardinia, Italy, May 13-15, 2010*. pp. 249–256.

Goodfellow, I., Bengio, Y. and Courville, A., 2016. *Deep Learning*. The MIT Press. ISBN 0262035618, 9780262035613.

Haller, G., 2015. "Lagrangian coherent structures". *Annual Review of Fluid Mechanics*, Vol. 47, pp. 137–162.

Juang, N. and Pappa, R.S., 1985. "An eigensystem realization algorithm for modal parameter identification and model reduction". *Journal of Guidance, Control, and Dynamics*, Vol. 8, pp. 620–627.

Kennedy, C.A., Carpenter, M.H. and Lewis, R.M., 1999. "Low-storage, explicit Runge-Kutta schemes for the compressible Navier-Stokes equations". ICASE Report No. 99-22.

Kingma, D.P. and Ba, J., 2014. "Adam: A method for stochastic optimization". *Proceedings of the 3rd International Conference on Learning Representations (ICLR)*. URL `http://arxiv.org/abs/1412.6980`.

Kutz, J., 2017. "Deep learning in fluid dynamics". *Journal of Fluid Mechanics*, Vol. 814, pp. 1–4.

Lele, S.K., 1992. "Compact finite difference schemes with spectral-like resolution". *Journal of Computational Physics*, Vol. 103, No. 1, pp. 16–42. ISSN 0021-9991.

Lumley, J.L., 1967. "The structure of inhomogeneous turbulence". In *Atmospheric Turbulence and Wave Propagation*, Nauka, Moscow, pp. 166–178.

Nagarajan, S., Lele, S.K. and Ferziger, J.H., 2003. "A robust high-order compact method for large eddy simulation". *Journal of Computational Physics*, Vol. 191, No. 2, pp. 392–419. ISSN 0021-9991.

Ribeiro, J.H.M. and Wolf, W.R., 2017. "Identification of coherent structures in the flow past a naca0012 airfoil via proper orthogonal decomposition". *Physics of Fluids (*submitted at *May 17, 2017)*.

Rowley, C.W., Colonius, T. and Murray, R.M., 2004. "Model reduction for compressible flows using {POD} and galerkin projection". *Physica D: Nonlinear Phenomena*, Vol. 189, No. 1-2, pp. 115 – 129.

Schmid, P.J., 2010. "Dynamic mode decomposition of numerical and experimental data". *Journal of Fluid Mechanics*, Vol. 656, p. 5âĂŞ28.

Sieber, M., Paschereit, C.O. and Oberleithner, K., 2016. "Spectral proper orthogonal decomposition". *Journal of Fluid Mechanics*, Vol. 792, pp. 798–828.

Taira, K., Brunton, S.L., Dawson, S.T.M., Rowley, C.W., Colonius, T., McKeon, B.J., Schmidt, O.T., Gordeyev, S., Theofilis, V. and Ukeiley, L.S., 2017. "Modal analysis of fluid flows: An overview". *AIAA Journal*, Vol. 47, pp. 1–28.

Wolf, W.R., Azevedo, J.L.F. and Lele, S.K., 2012a. "Convective effects and the role of quadrupole sources for aerofoil aeroacoustics". *Journal of Fluid Mechanics*, Vol. 708, pp. 502–538. ISSN 1469-7645.

Wolf, W.R., Lele, S.K., Jothiprasard, G. and Cheung, L., 2012b. "Investigation of noise generated by a du96 airfoil". In *18th AIAA/CEAS Aeroacoustics Conference (33th AIAA Aeroacoustics Conference)*.

8. RESPONSIBILITY NOTICE

The authors Hugo F. S. Lui and William R. Wolf are the only responsible for the printed material included in this paper.